



## **An Introduction to Compressible Flow for Propulsion Applications**

Antonio L. Sánchez

MAE, UCSD

January 2017

## Preface

The following notes are intended as a short introduction to Compressible Flow to be used in connection with 113 (Fundamentals of Propulsion)

# Contents

<b>1</b>	<b>Ideal Gas Flow</b>	<b>1</b>
	The Navier-Stokes equations . . . . .	1
	The speed of sound . . . . .	2
	The Mach number . . . . .	2
	Steady gas flow around a sphere . . . . .	3
	The Euler equations . . . . .	4
	Quasi-steady flow . . . . .	5
	Steady ideal flow of a gas: stagnation flow properties . . . . .	6
<b>2</b>	<b>Shock and Expansion Waves</b>	<b>9</b>
	Jump conditions across discontinuity surfaces . . . . .	9
	Normal discontinuities . . . . .	10
	Jump conditions across shock waves . . . . .	13
	Oblique shocks . . . . .	16
	Prandtl-Meyer expansions . . . . .	20
<b>3</b>	<b>Nozzle Flow</b>	<b>25</b>
	Quasisteady ideal gas flow in pipes . . . . .	25
	Subsonic and supersonic flow in pipes . . . . .	26
	Critical magnitudes . . . . .	27
	Flow in a convergent nozzle . . . . .	27
	Flow in convergent-divergent nozzles . . . . .	30



# List of figures

1.1	Perturbation regions for subsonic and supersonic flows. . . . .	2
1.2	Steady gas motion around a sphere. . . . .	3
2.1	Jumps across a discontinuity surface. . . . .	10
2.2	Hugoniot curve and Rayleigh line. . . . .	12
2.3	Velocity jumps across a normal discontinuity. . . . .	14
2.4	Piston-supported shock wave. . . . .	15
2.5	The variation of $\beta$ with $\delta$ for constant values of $M_1$ . . . . .	17
2.6	The variation of $p_2/p_1$ with $M_1$ for constant values of $M_2$ and $\delta$ . . . . .	18
2.7	Supersonic flow over a wedge. . . . .	20
2.8	Supersonic flow over a blunt body. . . . .	21
2.9	Supersonic flow over a concave wall. . . . .	22
2.10	Supersonic flow over a convex wall. . . . .	23
2.11	Differential evolution across a Mach wave. . . . .	24
2.12	Supersonic stream discharging to the vacuum. . . . .	24
3.1	The variation of the exit Mach number $M(L)$ and mass flow rate $G$ with $p_c/p_a$ as obtained from (3.16) and (3.17) for $\gamma = 1.4$ . . . . .	28
3.2	Pressure and Mach number distributions along a nozzle for different values of $p_a/p_c$ . . . . .	29
3.3	Flow in a convergent-divergent nozzle. . . . .	31

# Chapter 1

## Ideal Gas Flow

### The Navier-Stokes equations

To study the motion of a perfect gas, the conservation equations of continuity

$$\frac{\partial \rho}{\partial t} + \nabla \cdot (\rho \bar{v}) = 0, \quad (1.1)$$

momentum

$$\rho \frac{D\bar{v}}{Dt} = -\nabla p + \nabla \cdot \bar{\tau}' + \rho \bar{f}_m, \quad (1.2)$$

and energy

$$\rho \frac{De}{Dt} = -p \nabla \cdot \bar{v} + \bar{\tau}' : \nabla \bar{v} - \nabla \cdot \bar{q}, \quad (1.3)$$

must be supplemented with the equations of state

$$\rho = \frac{p}{R_g T} \quad \text{and} \quad e = e_o + c_v T \quad (1.4)$$

together with the constitutive equations

$$\bar{\tau}' = \mu(\nabla \bar{v} + \nabla \bar{v}^T) + (\mu_B - \frac{2}{3}\mu)(\nabla \cdot \bar{v})\bar{\mathbf{I}} \quad \text{and} \quad \bar{q} = -k \nabla T \quad (1.5)$$

and associated state functions

$$\mu = \mu(T), \quad \mu_B = \mu_B(T) \quad \text{and} \quad k = k(T). \quad (1.6)$$

The energy equation (1.3), which is written for a non-radiative chemically frozen gas, can be alternatively expressed in terms of the enthalpy  $h = e + p/\rho$  to give

$$\rho \frac{Dh}{Dt} - \frac{Dp}{Dt} = \bar{\tau}' : \nabla \bar{v} - \nabla \cdot \bar{q}, \quad (1.7)$$

and also in terms of the entropy, defined from  $Tds = dh - dp/\rho$ , yielding

$$\rho T \frac{Ds}{Dt} = \bar{\tau}' : \nabla \bar{v} + \nabla \cdot (k \nabla T). \quad (1.8)$$

The thermal equations of state can be written for the enthalpy and entropy as

$$h = e_o + c_p T \quad \text{and} \quad \frac{s - s_o}{c_v} = \ln \left( \frac{p}{\rho^\gamma} \right), \quad (1.9)$$

where  $c_v$  and  $c_p$  are the specific heat at constant volume and at constant pressure for the gas, with  $\gamma = c_p/c_v$ . According to (1.9), a flow is effectively isentropic when the entropy variations that appear  $\Delta s$  are much smaller than the corresponding specific heat.

## The speed of sound

Besides the enthalpy and the entropy, another thermodynamic quantity of interest in fluid-flow analysis is the speed of sound,  $a$ , which is the velocity at which the small pressure perturbations propagate in a compressible medium at rest, to be computed according to

$$a^2 = \left( \frac{\partial p}{\partial \rho} \right)_s. \quad (1.10)$$

For a perfect gas, straightforward differentiation of the second equation in (1.9) leads to

$$a = (\gamma p / \rho)^{1/2} = (\gamma R_g T)^{1/2}, \quad (1.11)$$

indicating that the speed of sound is a function of the temperature. The reader can verify that for air at  $T = 300$  K the above expression yields  $a \simeq 340$  m/s.

## The Mach number

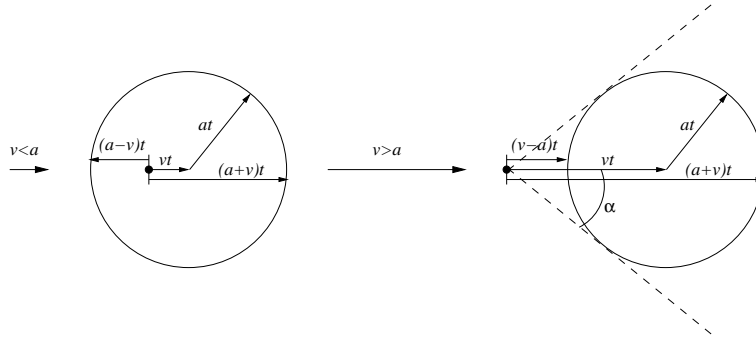


Figure 1.1: Perturbation regions for subsonic and supersonic flows.

Compressibility effects associated with the fluid motion are characterized by the Mach number

$$M = \frac{v}{a}, \quad (1.12)$$

defined as the ratio of the velocity magnitude  $v = |\vec{v}|$  to the speed of sound  $a$ . Flows can be subsonic, sonic or supersonic if the value of the Mach number is  $M < 1$ ,  $M = 1$ , or  $M > 1$ ,

respectively. Since the perturbations move with respect to the flow with the speed of sound, subsonic and supersonic flow show markedly different behaviors, as sketched in Fig. 1. As can be seen, a perturbation in a subsonic flow ends up affecting all of the flow field, because it propagates upstream sufficiently fast to overcome convection. In supersonic flow, however, convection sweeps downstream the perturbation, which affects only a conical region (termed the “Mach cone”) of semi-angle  $\alpha$  such that  $\sin(\alpha) = 1/M$ .

## Steady gas flow around a sphere

To compute a given flow field one needs to integrate (1.1) and (1.2) together with one of the alternative forms of the energy equation - i.e., (1.3), (1.7), or (1.8) - with appropriate initial and boundary conditions. To begin to introduce some needed concepts, it is of interest to consider, as an illustrative example, the steady buoyancy-free motion of a gas around a sphere of radius  $R$  with negligible radiation and chemical reaction. The ambient conditions in this case are given by  $\bar{v} = U_\infty \bar{e}_x$ ,  $T = T_\infty$ , and  $p = p_\infty$  whereas on the sphere surface we find  $\bar{v} = 0$  and  $T = T_w$ , where  $T_w$  is assumed to be constant.

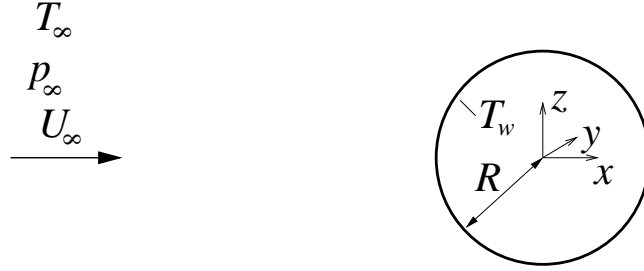


Figure 1.2: Steady gas motion around a sphere.

In this case, the problem reduces to that of integrating

$$\nabla \cdot (\rho \bar{v}) = 0 \quad (1.13)$$

$$\underbrace{\rho \bar{v} \cdot \nabla \bar{v}}_{\rho_\infty U_\infty^2 / R} = \underbrace{-\nabla p}_{\Delta p / R} + \underbrace{\nabla \cdot \bar{\tau}'}_{\mu U_\infty / R^2} \quad (1.14)$$

$$\underbrace{\rho T \bar{v} \cdot \nabla s}_{\rho_\infty T_\infty U_\infty \Delta s / R} = \underbrace{\bar{\tau}' : \nabla \bar{v}}_{\mu U_\infty^2 / R^2} + \underbrace{\nabla \cdot (k \nabla T)}_{k \Delta T / R^2} \quad (1.15)$$

supplemented with the constitutive law for  $\bar{\tau}'$  given in (1.5) and with the equations of state

$$\rho = \frac{p}{R_g T} \quad \text{and} \quad \frac{s - s_\infty}{c_v} = \ln \left( \frac{p/p_\infty}{(\rho/\rho_\infty)^\gamma} \right) \quad (1.16)$$

and subject to the boundary conditions

$$\begin{cases} |\bar{x}| = R : & \bar{v} = 0, \quad T = T_w \\ |\bar{x}| \gg R : & \bar{v} = U_\infty \bar{e}_x, \quad T = T_\infty, \quad p = p_\infty. \end{cases} \quad (1.17)$$



Note that, for convenience, the thermal equation of state in (1.16) has been written using the ambient conditions for the arbitrary reference state.

The estimated orders of magnitude are given below each term in the momentum and energy equations. The character of the solution depends on the value of the Reynolds number

$$Re = \frac{O(\rho \bar{v} \cdot \nabla \bar{v})}{O(\bar{\tau}')} = \frac{\rho_\infty U_\infty R}{\mu}. \quad (1.18)$$

When  $Re \gg 1$ , the viscous forces are found to be negligible in most of the flow field. The simplified balance equation that appears can be used to estimate the characteristic value of the spatial pressure differences appearing across the flow field according to

$$\underbrace{\rho \bar{v} \cdot \nabla \bar{v}}_{\rho_\infty U_\infty^2/R} \sim \underbrace{-\nabla p}_{\Delta p/R} \rightarrow \Delta p = \rho_\infty U_\infty^2. \quad (1.19)$$

It is of interest to compare these differences with the ambient value  $p_\infty$  according to

$$\frac{\Delta p}{p_\infty} = \frac{\rho_\infty U_\infty^2}{p_\infty} = \gamma \left( \frac{U_\infty}{a_\infty} \right)^2 = \gamma M_\infty^2. \quad (1.20)$$

As can be seen, the compressibility ratio  $\Delta p/p_\infty$  is proportional to the square of the Mach number

$$M_\infty = U_\infty/a_\infty. \quad (1.21)$$

Appreciable compressibility effects appear in flows with  $M_\infty \gtrsim 1$ , whereas in flows with  $M_\infty \ll 1$  the resulting spatial pressure differences are much smaller than the ambient pressure. In the latter case, one may rewrite the equation of state given in (1.16) in the simplified form  $p_\infty = \rho R_g T$ . According to the energy equation (1.15) the entropy of a fluid particle crossing the flow field changes due to the effects of viscous dissipation and thermal heat conduction. The corresponding characteristic entropy increase due to each separate effect,  $(s - s_\infty)_\phi$  and  $(s - s_\infty)_k$ , can be estimated by order-of-magnitude comparisons according to

$$\underbrace{\rho T \bar{v} \cdot \nabla s}_{\rho_\infty T_\infty U_\infty (s - s_\infty)_\phi/R} \sim \underbrace{\bar{\tau}' : \nabla \bar{v}}_{\mu U_\infty^2/R^2} \rightarrow \frac{(s - s_\infty)_\phi}{c_v} = \gamma(\gamma - 1) \frac{M_\infty^2}{Re} \quad (1.22)$$

and

$$\underbrace{\rho T \bar{v} \cdot \nabla s}_{\rho_\infty T_\infty U_\infty (s - s_\infty)_k/R} \sim \underbrace{\nabla \cdot (k \nabla T)}_{k \Delta T/R^2} \rightarrow \frac{(s - s_\infty)_k}{c_v} = \frac{\gamma}{Pr} \frac{\Delta T}{T_\infty} \frac{1}{Re}. \quad (1.23)$$

where  $Pr = \mu c_p/k$  is the Prandtl number ( $Pr = 0.7$  for air). The above expressions clearly indicate that when the Reynolds number is large the resulting flow is effectively isentropic, thereby reducing (1.15) to  $s = s_\infty$ .

## The Euler equations

According to the previous discussion, the effects of molecular transport, including viscous forces, heat conduction and also viscous dissipation, can be neglected in the first approximation whenever the condition  $Re \gg 1$  is satisfied, where  $Re = \rho_c v_c L_c / \mu_c$  is the Reynolds number of the

problem, defined from the characteristic values of the density and viscosity,  $\rho_c$  and  $\mu_c$ , velocity  $v_c$ , and length  $L_c$ <sup>1</sup>. The simplified set of conservation equations, called the Euler equations, is given by

$$\frac{\partial \rho}{\partial t} + \nabla \cdot (\rho \bar{v}) = 0, \quad (1.24)$$

$$\rho \left( \frac{\partial \bar{v}}{\partial t} + \bar{v} \cdot \nabla \bar{v} \right) = \rho \frac{D\bar{v}}{Dt} = -\nabla p + \rho \bar{f}_m, \quad (1.25)$$

$$\rho T \left( \frac{\partial s}{\partial t} + \bar{v} \cdot \nabla s \right) = \rho T \frac{Ds}{Dt} = 0. \quad (1.26)$$

This last equation indicates that the entropy of each fluid particle remains constant in the flow evolution. We say that the flow is **isentropic**. If at the initial instant all fluid particles have the same value of  $s$ , then in the subsequent evolution the entropy will remain uniform in the flow field, so that  $\nabla s = 0$ ; when this happens, the flow is said to be **homentropic**.

For the integration of (1.24)–(1.26), one needs to provide initial conditions, given by the initial values of the velocity and thermodynamic state at every point of the integration domain. Because of the absence of the second-order spatial derivatives, the Euler equations cannot however satisfy all of the boundary conditions. For the aerodynamic problem of flow around a body the subset of boundary conditions to be satisfied by the Euler equations (1.24)–(1.26) include those far from the body, i.e.,  $\bar{v} = U_\infty \bar{e}_x$ ,  $p = p_\infty$ , and  $T = T_\infty$  at  $|\bar{x}| \gg R$ . On the body surface, however, we cannot impose either the temperature or the velocity, so that integration of (1.24)–(1.26) provides in general a solution with  $T \neq T_w$  and  $\bar{v} \neq 0$  on the body surface  $|\bar{x}| = R$ . For the velocity, the presence of the pressure forces in the momentum equation prevents the fluid from penetrating the solid surface, so that the resulting velocity component normal to the wall is strictly zero, that is, for integrating (1.24)–(1.26) we must impose  $\bar{v} \cdot \bar{n} = 0$  on the body surface.

## Quasi-steady flow

For a flow with characteristic length  $L_c$ , characteristic velocity  $v_c$ , and characteristic time of flow variation  $t_c$ , the importance of the unsteady terms in the conservation equations is measured through the so-called Strouhal number  $St$ , which compares the orders of magnitude of the unsteady and convective terms according to

$$St = \frac{O(\partial \rho / \partial t)}{O(\nabla \cdot (\rho \bar{v}))} = \frac{O(\partial \bar{v} / \partial t)}{O(\bar{v} \cdot \nabla \bar{v})} = \frac{O(\partial s / \partial t)}{O(\bar{v} \cdot \nabla s)} = \frac{L_c / v_c}{t_c}. \quad (1.27)$$

For a given problem, the values of  $L_c$ ,  $v_c$ , and  $t_c$  can be estimated from the boundary conditions. For instance, for flow of a fluid stream of variable velocity  $U_\infty(t)$  (e.g.,  $U_\infty = U_o \sin \Omega t$ ) around a body (e.g., a sphere), the value of  $L_c$  will be given by the characteristic body size (e.g., the

<sup>1</sup>Note that, regardless of the value of the Reynolds number, molecular transport is also negligible in unsteady flows when the condition

$$\frac{\rho_c L_c^2}{\mu_c t_c} \gg 1$$

is satisfied, where  $t_c$  is the characteristic time of flow variation. Under those conditions, the molecular-transport terms are found to be negligible compared with the unsteady terms, so that, for instance,  $\rho \partial \bar{v} / \partial t \gg \nabla \cdot \bar{\tau}'$  in the momentum conservation equation.

sphere radius  $R$ ), whereas the values of  $v_c$  and  $t_c$  will be the characteristic free-stream velocity (e.g., its mean value  $v_c = U_o$ ) and the characteristic time of free-stream velocity variation (e.g.,  $t_c = \Omega^{-1}$ ).

Flows with  $St \ll 1$  are said to be **quasi-steady**, in that, for their description, one may in the first approximation neglect the time derivatives in the conservation equations, which therefore become

$$\nabla \cdot (\rho \bar{v}) = 0, \quad (1.28)$$

$$\rho \bar{v} \cdot \nabla \bar{v} = -\nabla p + \rho \bar{f}_m, \quad (1.29)$$

$$\bar{v} \cdot \nabla s = 0. \quad (1.30)$$

The flow is termed quasi-steady, as opposed to strictly steady, because the resulting solution depends on the time through the slowly-varying boundary conditions. For instance, for the sphere example with variable free-stream velocity, when  $St = R\Omega/U_o \ll 1$  the instantaneous velocity field around the sphere  $\bar{v}(\bar{x}, t)$  will be that corresponding to steady motion with free-stream velocity  $U_\infty = U_o \sin \Omega t$ . Note that the condition  $St \ll 1$  implies that the fluid-particle residence time  $L_c/v_c$  is much smaller than the time required to change appreciably the boundary conditions, so that the boundary conditions remain almost constant during the time that it takes each fluid particle to cross the flow field. As a result, each individual fluid particle behaves as though the flow were steady, with the values of the boundary conditions corresponding to the instant of time at which they cross the flow field.

## Steady ideal flow of a gas: stagnation flow properties

When the mass forces are conservative, i.e.,  $\bar{f}_m = -\nabla U$ , we may rewrite (1.29) in the form

$$\bar{v} \cdot \nabla \bar{v} = -\frac{\nabla p}{\rho} - \nabla U. \quad (1.31)$$

The projection of this vector equation along a given stream line, obtained by scalar multiplication by  $\bar{v}/v$  with use of the identity  $\bar{v} \cdot \nabla \bar{v} = \nabla(v^2/2) - \bar{v} \wedge (\nabla \wedge \bar{v})$ , yields

$$\frac{\partial}{\partial l} (v^2/2 + U) + \frac{1}{\rho} \frac{\partial p}{\partial l} = 0, \quad (1.32)$$

where

$$\frac{\partial}{\partial l} = \frac{\bar{v}}{v} \cdot \nabla \quad (1.33)$$

denotes the derivative along stream lines.

According to (1.30),

$$\frac{\partial s}{\partial l} = 0, \quad (1.34)$$

i.e. the entropy is constant along stream lines, with a value

$$s = s_0, \quad (1.35)$$

that may be different for different stream lines and may also vary slowly with time. This last result can be used to simplify the description of steady gas flow at large Reynolds numbers. Using the definition of entropy  $Tds = dh - dp/\rho$  along with (1.34) yields

$$\frac{\partial h}{\partial l} = \frac{1}{\rho} \frac{\partial p}{\partial l}, \quad (1.36)$$

which can be substituted into (1.32) to give

$$\frac{\partial}{\partial l} \left( h + \frac{v^2}{2} + U \right) = 0. \quad (1.37)$$

In many gas-flow applications mass forces have a negligible effect on the gas motion, because the velocity is sufficiently large for the associated Froude number to satisfy

$$Fr = \frac{O(\rho \bar{v} \cdot \nabla \bar{v})}{O(\rho \bar{f}_m)} = \frac{v_c^2}{L_c \bar{f}_{m_c}} \gg 1. \quad (1.38)$$

When this condition is satisfied, then (1.37) indicates that

$$h + \frac{v^2}{2} = h_0, \quad (1.39)$$

is constant along a given stream line. For known values of  $s_0$  and  $h_0$ , the equations (1.35) and (1.39) together with the equations of state

$$T = T(s, h), \quad p = p(s, h), \quad \rho = \rho(s, h), \quad \text{and} \quad a = a(s, h) \quad (1.40)$$

enable the computation of the values of  $s$ ,  $h$ ,  $T$ ,  $p$ ,  $\rho$ , and  $a$  in terms of the local value of the flow velocity  $v$ . The constants  $s_0$  and  $h_0$  together with the corresponding values  $T_0$ ,  $p_0$ ,  $\rho_0$ , and  $a_0$ , obtained by substituting the values  $s_0$  and  $h_0$  in the equations of state (1.40), are called stagnation flow properties. The explicit form of the equations of state for a perfect gas, given above in (1.4), (1.9), and (1.11), can be used to express the different stagnation flow properties in terms of the local Mach number according to

$$\frac{h_0}{h} = \frac{T_0}{T} = \left( \frac{a_0}{a} \right)^2 = \left( \frac{p_0}{p} \right)^{(\gamma-1)/\gamma} = \left( \frac{\rho_0}{\rho} \right)^{\gamma-1} = 1 + \frac{\gamma-1}{2} M^2. \quad (1.41)$$

For **steady** (or quasi-steady) **ideal gas flow** with **negligible body forces**, the values of  $s_0$ ,  $h_0$ ,  $T_0$ ,  $a_0$ ,  $p_0$ , and  $\rho_0$  remain constant along a given stream line and (1.41) can be employed to compute  $h$ ,  $T$ ,  $a$ ,  $p$ , and  $\rho$  as a function of the local value of the Mach number  $M$ . For  $M \ll 1$ , equation (1.41) indicates that the gas moves with small variations of the temperature, density, and pressure. The latter can be computed by expanding

$$\frac{p_0}{p} = \left( 1 + \frac{\gamma-1}{2} M^2 \right)^{\gamma/(\gamma-1)} \quad (1.42)$$

for  $M \ll 1$  to give the familiar Bernoulli's equation

$$p + \rho_0 v^2 / 2 = p_0, \quad (1.43)$$

thereby illustrating the similarities between gas motion at low Mach numbers and liquid motion.



## Chapter 2

# Shock and Expansion Waves

For the solution of the Euler equations to represent adequately a given large-Reynolds-number flow, we need to consider in general the existence of discontinuity surfaces, across which the fluid properties or their derivatives exhibit finite jumps. Mach cones, for instance, represent an example of weak discontinuities with jumps in derivatives. Boundary layers (and also vortex sheets and mixing layers) are examples of tangential discontinuities. We shall focus below on the analysis of normal discontinuities, showing that they are always compression waves, also called shock waves, with specific results given below for the jump conditions across normal and oblique shocks. Conversely, expansion waves cannot be discontinuities; rather, they are continuous isentropic waves, to be analyzed below in the specific case of steady flow around a sharp corner (the so-called Prandtl-Meyer expansion flow).

### Jump conditions across discontinuity surfaces

To determine the conditions that relate the different flow properties that exist on the sides of a given discontinuity surface we shall apply the conservation equations to the infinitesimally small control volume shown in figure 2.1. As can be seen, the control volume includes faces of area  $d\sigma$ , lying on the two sides of the surface, separated by a small distance  $\varepsilon$ . In a reference frame moving with the discontinuity, mass conservation can be expressed in the form

$$\frac{d}{dt} \int_{V_c} \rho dV + \int_{\Sigma_c} \rho \bar{v} \cdot \bar{n} d\sigma = 0. \quad (2.1)$$

The first integral is proportional to the volume of the control volume, of order  $\varepsilon d\sigma$ , and therefore becomes negligibly small when a infinitesimally thin control volume satisfying  $\varepsilon \ll (d\sigma)^{1/2}$  is considered. In that limit, only fluxes across the two faces of area  $d\sigma$  need to be computed when evaluating the second integral, which therefore provides the simplified continuity equation

$$\rho_1 v_{1n} = \rho_2 v_{2n} = m, \quad (2.2)$$

where  $m$  denotes the local value of the mass flux across the discontinuity and the subscript  $n$  is used to denote normal velocity components, with the subscript  $t$  employed below for the tangential components. Volume integrals can also be neglected when evaluating the momentum

and energy conservation equations, which can be seen to provide

$$\rho_1 v_{1n}^2 + p_1 = \rho_2 v_{2n}^2 + p_2 \quad (2.3)$$

$$\rho_1 v_{1n} v_{1t} = \rho_2 v_{2n} v_{2t} \quad (2.4)$$

and

$$m \left( e_1 + \frac{p_1}{\rho_1} + \frac{v_1^2}{2} \right) = m \left( e_2 + \frac{p_2}{\rho_2} + \frac{v_2^2}{2} \right). \quad (2.5)$$

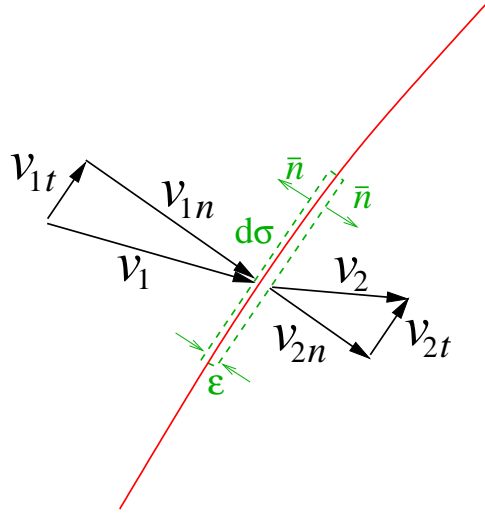


Figure 2.1: Jumps across a discontinuity surface.

Equations (2.2)–(2.5) apply to all discontinuities. Tangential discontinuities, such as boundary layers and vortex sheets, are defined by the condition that the mass flux is identically zero, that is,  $m = 0$ . From (2.2) it then follows that  $v_{1n} = v_{2n} = 0$  and, from (2.3), it is seen that  $p_1 = p_2$ , indicating that the jump in pressure across tangential discontinuities is zero, a condition used before when analyzing jets and boundary layers. With  $m = 0$ , the conservation of tangential momentum and energy, expressed in (2.4) and (2.5), are identically satisfied, regardless of the values of  $v_{1t} \neq v_{2t}$ ,  $\rho_1 \neq \rho_2$ , and  $T_1 \neq T_2$ .

## Normal discontinuities

When the mass flux across the discontinuity is nonzero, then it follows from (2.4) that

$$v_{1t} = v_{2t}, \quad (2.6)$$

whereas (2.5) reduces to

$$h_1 + \frac{v_1^2}{2} = h_2 + \frac{v_2^2}{2}, \quad (2.7)$$

indicating that, in a reference frame moving with the discontinuity, the stagnation enthalpy (and, therefore, the stagnation temperature) is conserved.

For given values of  $v_{1n}$ ,  $\rho_1$ , and  $p_1$ , equations (2.2), (2.3), and

$$\frac{\gamma}{\gamma-1} \frac{p_1}{\rho_1} + \frac{v_{1n}^2}{2} = \frac{\gamma}{\gamma-1} \frac{p_2}{\rho_2} + \frac{v_{2n}^2}{2} \quad (2.8)$$

determine  $v_{2n}$ ,  $\rho_2$ , and  $p_2$ , with (2.8) corresponding to the energy conservation balance (2.7) written with use made of (2.6) and of the thermodynamic identity  $h = [\gamma/(\gamma-1)]p/\rho$ .

Straightforward manipulation of (2.2) and (2.3) leads to the equation of the so-called Rayleigh line

$$\frac{p_2}{p_1} - 1 = \frac{m^2}{\rho_1 p_1} \left( 1 - \frac{\rho_1}{\rho_2} \right). \quad (2.9)$$

On the other hand, writing (2.8) in the form

$$\frac{\gamma}{\gamma-1} \left( \frac{p_2}{\rho_2} - \frac{p_1}{\rho_1} \right) = \frac{1}{2} (v_{1n}^2 - v_{2n}^2) = \frac{1}{2} m^2 \left( \frac{1}{\rho_1} - \frac{1}{\rho_2} \right) \left( \frac{1}{\rho_1} + \frac{1}{\rho_2} \right) \quad (2.10)$$

and using (2.9) to eliminate  $m^2$  yields

$$\frac{p_2}{p_1} = \frac{\frac{\gamma+1}{\gamma-1} - \frac{\rho_1}{\rho_2}}{\frac{\gamma+1}{\gamma-1} \frac{\rho_1}{\rho_2} - 1}. \quad (2.11)$$

This last equation, relating the jumps in pressure and density across the discontinuity, is known as Hugoniot curve. Observation of the numerator and denominator in (2.11) indicates that the solution for the density ratio across the discontinuity must lie in the range

$$\frac{\gamma-1}{\gamma+1} < \frac{\rho_1}{\rho_2} < \frac{\gamma+1}{\gamma-1} \quad (2.12)$$

while the range of possible pressure ratios extends in principle for  $0 < p_2/p_1 < \infty$ , giving the solution shown in Fig. 2.2 for  $\gamma = 1.4$ .

For a given mass flux  $m$ , the values of  $p_2/p_1$  and  $\rho_1/\rho_2$  are determined by the point where the Rayleigh line (2.9) and the Hugoniot curve (2.11) cross in Fig. 2.2 (of course, a second solution  $p_2/p_1 = \rho_1/\rho_2 = 1$  always exists, but that is just the trivial solution corresponding to a continuous flow with no jumps).

To investigate the different possible solutions, we begin by noting that the slope of the Rayleigh line can be written in terms of the Mach number associated with the normal component of the incident velocity  $M_{1n} = v_{1n}/a_1$  according to

$$-\frac{m^2}{\rho_1 p_1} = -\frac{v_{1n}^2}{p_1/\rho_1} = -\gamma M_{1n}^2. \quad (2.13)$$

This value is to be compared with the slope of the Hugoniot curve at  $\rho_1/\rho_2 = 1$ , which can be computed by straightforward differentiation of (2.11) to give

$$\left( \frac{d(p_2/p_1)}{d(\rho_1/\rho_2)} \right)_{\rho_1/\rho_2=1} = -\gamma. \quad (2.14)$$

For  $M_{1n} = 1$  the Rayleigh line is tangent to the Hugoniot curve at  $p_2/p_1 = \rho_1/\rho_2 = 1$ , which is therefore the only solution of (2.9) and (2.11), whereas a nontrivial crossing point appears for  $M_{1n} \neq 1$  according to



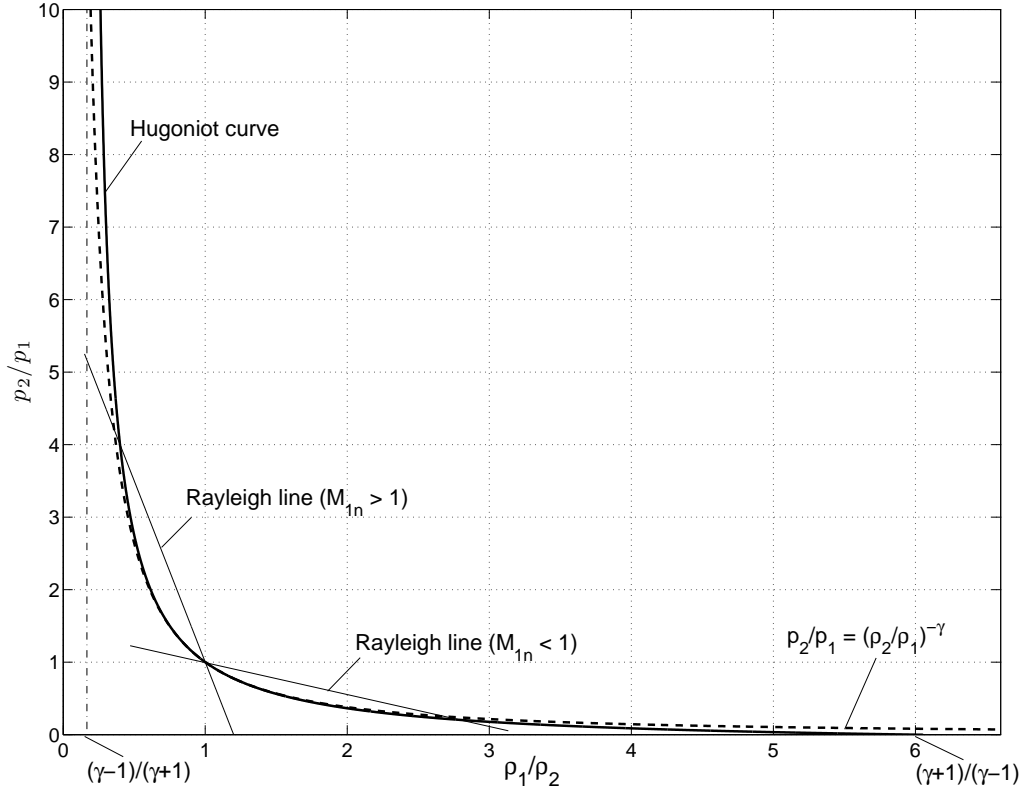


Figure 2.2: Hugoniot curve and Rayleigh line.

- If the normal component of the incident velocity is supersonic ( $M_{1n} > 1$ ), then the Rayleigh line crosses the Hugoniot curve along the upper stretch, so that the solution corresponds to a compression with

$$\infty > \frac{p_2}{p_1} > 1 \quad \text{and} \quad \frac{\gamma - 1}{\gamma + 1} < \frac{\rho_1}{\rho_2} < 1$$

- If the normal component of the incident velocity is subsonic ( $M_{1n} < 1$ ), then the Rayleigh line crosses the Hugoniot curve along the lower stretch, so that the solution corresponds to an expansion with

$$1 > \frac{p_2}{p_1} > 0 \quad \text{and} \quad 1 < \frac{\rho_1}{\rho_2} < \frac{\gamma + 1}{\gamma - 1}$$

Although both compressions and expansions are apparently valid solutions of (2.9) and (2.11), only compression waves, termed *shock waves*, may exist in reality. To prove this point, one may use thermodynamic arguments based on the second principle, which indicates that, in an adiabatic process, the entropy change  $s_2 - s_1$  can never be negative, i.e., the entropy can never

be destroyed. For a perfect gas,

$$\frac{s_2 - s_1}{c_v} = \ln \left( \frac{p_2/p_1}{(\rho_2/\rho_1)^\gamma} \right), \quad (2.15)$$

and one may use (2.11) to compute the entropy variation. As seen in Fig. 2.2, for  $\rho_1/\rho_2 < 1$  the Hugoniot curve (2.11) lies above the isentrope  $p_2/p_1 = (\rho_2/\rho_1)^\gamma$ . Compression waves, therefore, are associated with positive entropy increments

$$\frac{s_2 - s_1}{c_v} = \ln \left[ \frac{\left( \frac{\gamma+1}{\gamma-1} - \frac{\rho_1}{\rho_2} \right) / \left( \frac{\gamma+1}{\gamma-1} \frac{\rho_1}{\rho_2} - 1 \right)}{(\rho_2/\rho_1)^\gamma} \right] > 0, \quad (2.16)$$

as can be calculated from (2.15). Conversely, in expansion waves with  $\rho_1/\rho_2 < 1$  the Hugoniot curve (2.11) lies below the isentrope  $p_2/p_1 = (\rho_2/\rho_1)^\gamma$ , so that the entropy change computed from (2.15) would be negative ( $s_2 - s_1 < 0$ ), thereby violating the second principle of thermodynamics.

Hence, normal discontinuity surfaces are always shock waves, with jumps of thermodynamic properties in the ranges

$$\infty > \frac{p_2}{p_1} > 1, \quad \frac{\gamma-1}{\gamma+1} < \frac{\rho_1}{\rho_2} < 1, \quad \text{and} \quad \infty > \frac{T_2}{T_1} > 1, \quad (2.17)$$

the latter to be computed from the equation of state  $T_2/T_1 = (p_2/p_1)/(\rho_2/\rho_1)$ . The normal component of the incident velocity  $v_{1n}$  must be supersonic, so that the inequalities

$$M_1 > M_{1n} > 1 \quad (2.18)$$

are always satisfied. Use of (2.3) and (2.6) leads to the additional conditions

$$\frac{\gamma-1}{\gamma+1} < \frac{v_{2n}}{v_{1n}} < 1 \quad \text{and} \quad \frac{v_2}{v_1} < 1. \quad (2.19)$$

It can also be seen that

$$M_{2n} < 1. \quad (2.20)$$

It should be noted that, despite this last result, in oblique shock waves the downstream velocity can be however supersonic, i.e.,  $M_2 > 1$ .

## Jump conditions across shock waves

To resolve for the jumps across a generic shock wave, it is convenient to consider first the change in the normal component of the velocity along with the jumps in thermodynamic properties, and address subsequently the deflection of the flow  $\delta$  as a function of the incident angle  $\beta$  (see Fig. 2.3). The development begins by using (2.2), (2.3), and (2.8), which are rewritten below for convenience

$$\rho_1 v_{1n} = \rho_2 v_{2n}, \quad (2.21)$$

$$\rho_1 v_{1n}^2 + p_1 = \rho_2 v_{2n}^2 + p_2, \quad (2.22)$$

$$\frac{\gamma}{\gamma-1} \frac{p_1}{\rho_1} + \frac{v_{1n}^2}{2} = \frac{\gamma}{\gamma-1} \frac{p_2}{\rho_2} + \frac{v_{2n}^2}{2}. \quad (2.23)$$

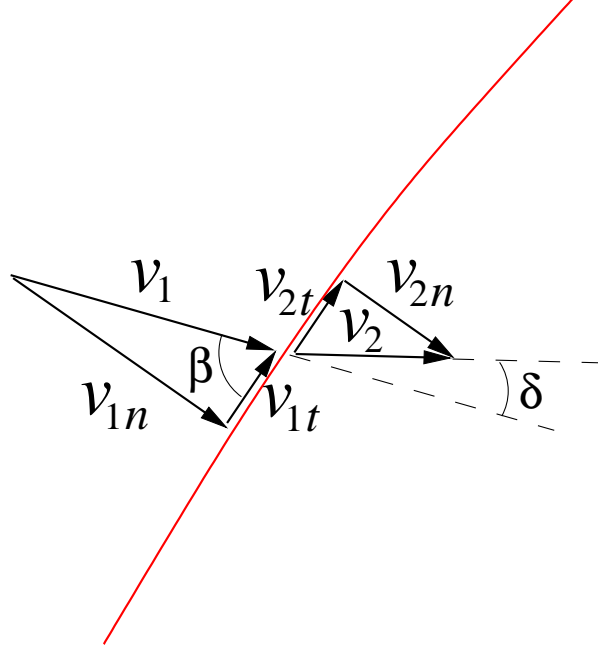


Figure 2.3: Velocity jumps across a normal discontinuity.

For a gas of known specific-heat ratio  $\gamma$ , these three equations determine the downstream values  $v_{2n}$ ,  $p_2$ , and  $\rho_2$  in terms of  $v_{1n}$ ,  $p_1$ , and  $\rho_1$ . The dependence can be simplified by using the  $\Pi$  theorem of dimensional analysis to give

$$\left. \begin{aligned} v_{2n} &= f_1(v_{1n}, p_1, \rho_1, \gamma) \\ p_2 &= f_2(v_{1n}, p_1, \rho_1, \gamma) \\ \rho_2 &= f_3(v_{1n}, p_1, \rho_1, \gamma) \end{aligned} \right\} \Rightarrow \left\{ \begin{aligned} v_{2n}/v_{1n} &= \varphi_1(M_{1n}, \gamma) \\ p_2/p_1 &= \varphi_2(M_{1n}, \gamma) \\ \rho_2/\rho_1 &= \varphi_3(M_{1n}, \gamma) \end{aligned} \right. \quad (2.24)$$

The functions  $\varphi_1$ ,  $\varphi_2$ , and  $\varphi_3$  can be determined by manipulation of (2.21)–(2.23) to give (we leave the needed development as an exercise for the reader)

$$\frac{v_{2n}}{v_{1n}} = \left( \frac{\rho_2}{\rho_1} \right)^{-1} = \frac{2 + (\gamma - 1)M_{1n}^2}{(\gamma + 1)M_{1n}^2} \quad \text{and} \quad \frac{p_2}{p_1} = \frac{2\gamma M_{1n}^2 + 1 - \gamma}{\gamma + 1}, \quad (2.25)$$

which can be combined with  $T_2/T_1 = (p_2/p_1)/(\rho_2/\rho_1)$  and  $M_{2n}^2 = M_{1n}^2(\rho_2/\rho_1)^{-1}(p_2/p_1)^{-1}$  to give

$$\frac{T_2}{T_1} = \frac{(2\gamma M_{1n}^2 + 1 - \gamma)[2 + (\gamma - 1)M_{1n}^2]}{(\gamma + 1)^2 M_{1n}^2} \quad \text{and} \quad M_{2n}^2 = \frac{2 + (\gamma - 1)M_{1n}^2}{2\gamma M_{1n}^2 + 1 - \gamma}. \quad (2.26)$$

The above formulae take simplified forms in limiting cases of interest, including very strong shocks with  $M_{1n} \gg 1$ , for which

$$\frac{v_{2n}}{v_{1n}} = \left( \frac{\rho_2}{\rho_1} \right)^{-1} = \frac{\gamma - 1}{\gamma + 1}, \quad \frac{p_2}{p_1} = \frac{2\gamma M_{1n}^2}{\gamma + 1}, \quad \frac{T_2}{T_1} = \frac{2\gamma(\gamma - 1)M_{1n}^2}{(\gamma + 1)^2} \quad \text{and} \quad M_{2n}^2 = \frac{\gamma - 1}{2\gamma}, \quad (2.27)$$

and weak shocks with  $\varepsilon = M_{1n} - 1 \ll 1$ , for which

$$\frac{v_{2n}}{v_{1n}} = \left(\frac{\rho_2}{\rho_1}\right)^{-1} = 1 - \frac{2\varepsilon}{\gamma + 1}, \quad \frac{p_2}{p_1} = 1 + \frac{2\gamma\varepsilon}{\gamma + 1}, \quad \frac{T_2}{T_1} = 1 + \frac{2(\gamma - 1)\varepsilon}{\gamma + 1} \quad (2.28)$$

and  $1 - M_{2n} = \varepsilon$ . The associated entropy increase can be computed from (2.15) to give  $(s_2 - s_1)/c_v \sim \varepsilon^3$ , indicating that these weak shocks are nearly isentropic.

For normal shock waves, such that the incident flow forms an angle  $\beta = \pi/2$  with the shock, no flow deflection occurs, so that  $M_1 = M_{1n}$  and  $M_2 = M_{2n}$ , and the above equations (2.25) and (2.26) are all we need to determine the jumps across the shock. As an illustrative example, we can use them to determine the flow induced by a piston moving with constant velocity in a long cylindrical tube containing a gas. The piston, initially at rest, is suddenly accelerated to reach a constant velocity  $V_P$ , generating a shock wave that moves with velocity  $V_{SW}$  along the tube. The gas ahead of the shock is at rest, with initial thermodynamic properties characterized for instance by the sound velocity  $a_1$  and pressure  $p_1$ . The shock wave sets the fluid in motion, so that the gas between the shock and the piston moves with uniform constant velocity, equal to that of the piston.

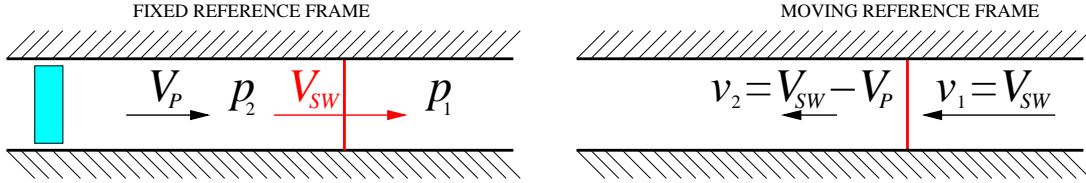


Figure 2.4: Piston-supported shock wave.

The velocities ahead and behind the shock  $v_1 = v_{1n}$  and  $v_2 = v_{2n}$  and the corresponding Mach numbers  $M_{1n}$  and  $M_{2n}$  appearing in (2.25) and (2.26) are measured relative to the shock, so in analyzing the problem we need to use a reference frame moving to the right with velocity  $V_{SW}$ . In that reference frame, the incident and downstream velocities are  $v_1 = V_{SW}$  and  $v_2 = V_{SW} - V_P$ , whereas the incident Mach number is  $M_{1n} = M_1 = V_{SW}/a_1$ . In terms of these quantities, the first equation in (2.25) yields

$$\frac{v_2}{v_1} = 1 - \frac{V_P}{V_{SW}} = \frac{2 + (\gamma - 1)(V_{SW}/a_1)^2}{(\gamma + 1)(V_{SW}/a_1)^2}, \quad (2.29)$$

which can be rewritten in the form

$$\left(\frac{V_{SW}}{a_1}\right)^2 - \frac{\gamma + 1}{2} \frac{V_P}{a_1} \left(\frac{V_{SW}}{a_1}\right) - 1 = 0. \quad (2.30)$$

Solving now for  $V_{SW}/a_1$  gives

$$M_{1n} = \frac{V_{SW}}{a_1} = \frac{\gamma + 1}{4} \frac{V_P}{a_1} + \left[1 + \left(\frac{\gamma + 1}{4}\right)^2 \left(\frac{V_P}{a_1}\right)^2\right]^{1/2}, \quad (2.31)$$

which can be used in (2.25) and (2.26) to determine the pressure, density and temperature in front of the piston as a function of  $V_P/a_1$ .

The above piston problem can be used as a simplified representation of the flow induced by a high-speed train entering a tunnel, the main simplification being that our piston occupies the whole transverse section of the tube, whereas in reality the train occupies only a fraction of the tunnel section. The results indicate that, as the train enters the tunnel, a sudden overpressure develops immediately ahead. The shock is weak for  $V_P \ll a_1$ , when

$$M_{1n} - 1 = \frac{\gamma + 1}{4} \frac{V_P}{a_1} \ll 1 \quad \text{and} \quad \frac{p_2}{p_1} - 1 = \frac{\gamma}{2} \frac{V_P}{a_1} \ll 1,$$

which explain why, in conventional trains, the problems encountered at the entrance of a tunnel are minor. Relative pressure differences of order unity appear however as  $V_P$  approaches values of the order of the sound velocity  $a_1$ . That is the case of high-speed trains, for which special measures need to be taken to remedy the overpressure problem at the tunnel entrance.

## Oblique shocks

For known values of  $M_1$  and  $\beta$  one may compute

$$M_{1n} = M_1 \sin \beta, \quad (2.32)$$

which in turn determines from (2.25) and (2.26) the jumps of thermodynamic properties and the values of

$$M_{2n}^2 = \frac{2 + (\gamma - 1)M_1^2 \sin^2 \beta}{2\gamma M_1^2 \sin^2 \beta + 1 - \gamma} \quad (2.33)$$

and

$$\frac{v_{2n}}{v_{1n}} = \frac{2 + (\gamma - 1)M_1^2 \sin^2 \beta}{(\gamma + 1)M_1^2 \sin^2 \beta}. \quad (2.34)$$

To determine the flow deflection, we use (2.6) written in the form

$$v_t = v_1 \cos(\beta) = v_2 \cos(\beta - \delta). \quad (2.35)$$

Using the equations  $v_{1n} = v_1 \sin(\beta)$  and  $v_{2n} = v_2 \sin(\beta - \delta)$  to give

$$\frac{\tan(\beta - \delta)}{\tan(\beta)} = \frac{v_{2n}}{v_{1n}} \quad (2.36)$$

and solving for  $\delta$  with use made of (2.34) yields

$$\tan(\delta) = 2 \cot(\beta) \frac{M_1^2 \sin^2(\beta) - 1}{2 + M_1^2[\gamma + \cos(2\beta)]}. \quad (2.37)$$

Once  $\delta$  is known one may easily compute

$$M_2 = \frac{M_{2n}}{\sin(\beta - \delta)}, \quad (2.38)$$

with  $M_{2n}$  determined from (2.33).

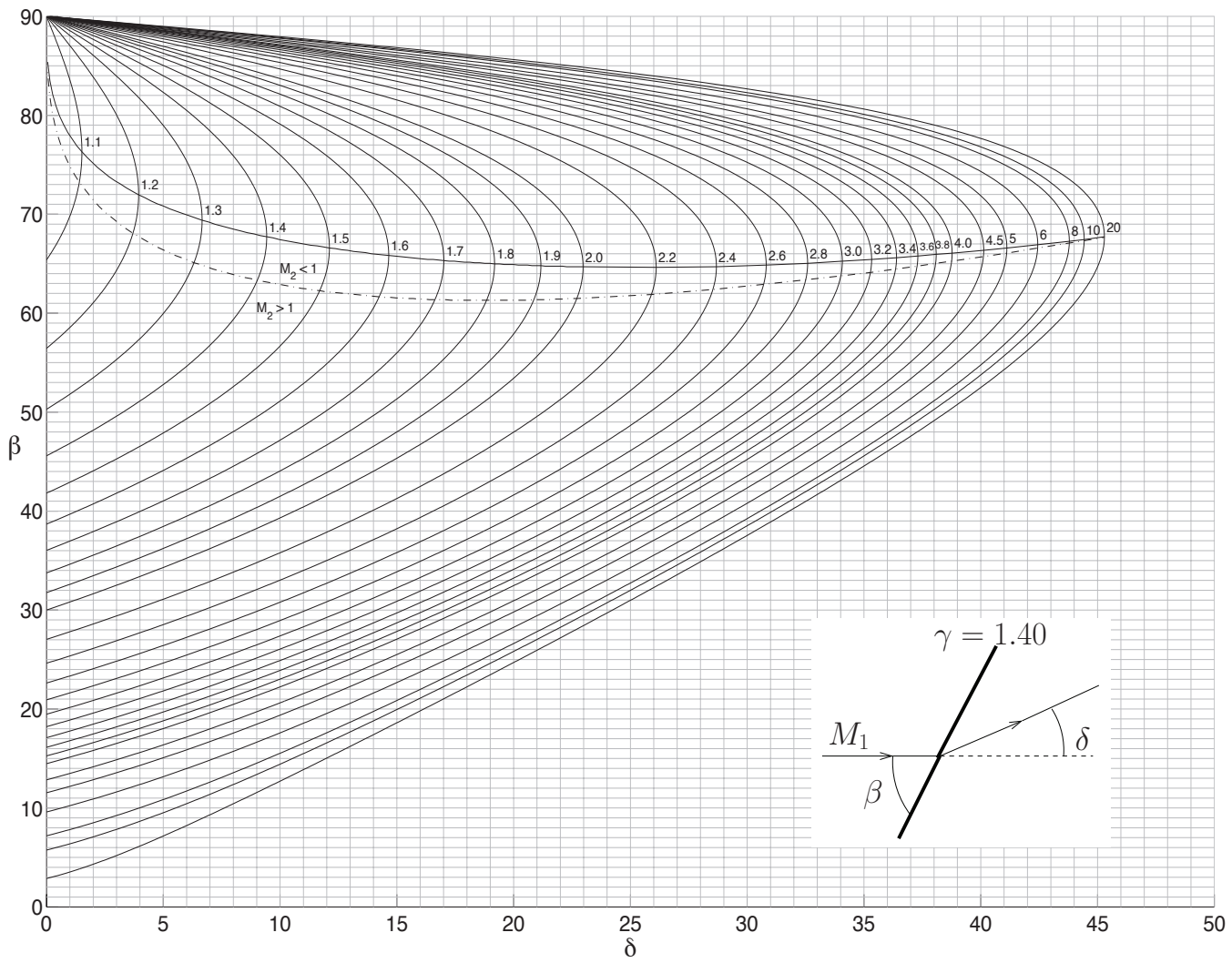


Figure 2.5: The variation of  $\beta$  with  $\delta$  for constant values of  $M_1$ .

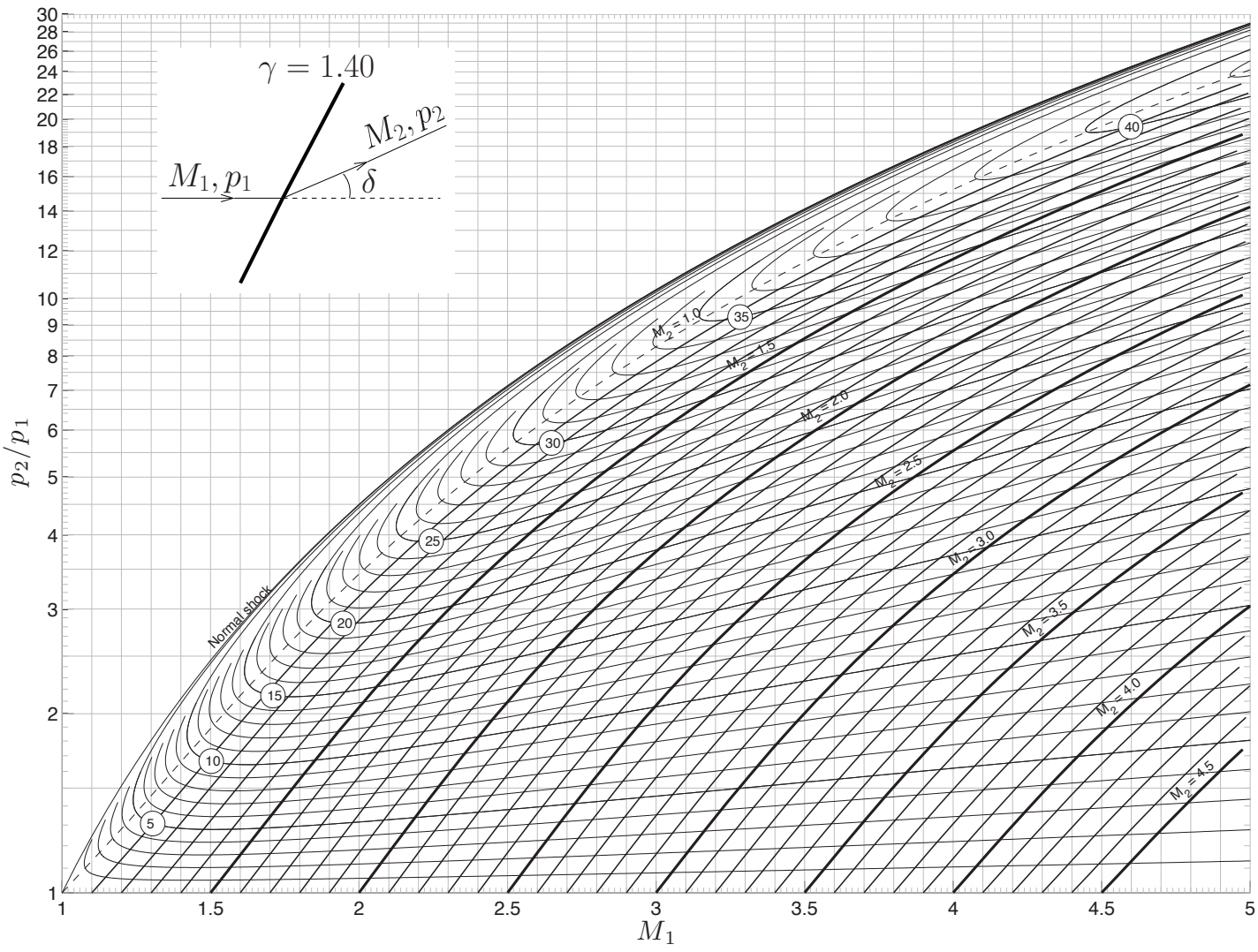


Figure 2.6: The variation of  $p_2/p_1$  with  $M_1$  for constant values of  $M_2$  and  $\delta$ .

The results are summarized in Figs. 2.5 and 2.6, where the angles are given in degrees. In particular, Fig. 2.5 indicates that for given values of  $M_1$  and  $\delta$  two different solutions are found if  $\delta < \delta_{\max}$  and no solution exists for  $\delta > \delta_{\max}$ , where the value of  $\delta_{\max}$  increases for increasing  $M_1$ . For  $\delta < \delta_{\max}$ , the solution with larger  $\beta$  corresponds to a stronger shock wave (i.e., larger value of  $M_{1n} = M_1 \sin \beta$ ). The corresponding value of  $M_{2n}$  is sufficiently small that the flow downstream is subsonic, that is,  $M_2 < 1$ . On the other hand, the solution lying along the lower part of the curve of constant  $M_1$  in Fig. 2.5 corresponds to a lower value of  $\beta$ , and therefore a weaker solution including a values of  $M_2$  that are generally supersonic (except for a small region near  $\delta = \delta_{\max}$ , as indicated in the figure). Because the associated downstream flow is supersonic, the weak-shock solution is more stable, in that perturbations can never reach it from downstream. Because of their stable character, when both strong or weak solutions may exist, weak solutions tend to prevail in realistic configurations.

For each value of  $M_1$ , there exist two solutions with zero deflection angle  $\delta = 0$ . One is the normal shock wave, corresponding to  $\beta = \pi/2$  and  $M_1 = M_{1n}$ , which is the strongest possible wave for that value of  $M_1$ . The other, corresponding to  $\beta = \mu$  with

$$\mu = \sin^{-1} \left( \frac{1}{M_1} \right), \quad (2.39)$$

is the weakest shock wave for that value of  $M_1$ ; the incident angle is such that  $M_{1n} = M_1 \sin \beta = 1$ . These limiting solutions are termed *Mach waves*. According to what we mentioned below (2.28), these weak shocks are effectively isentropic compressions. A Mach wave is seen to bound, for instance, the Mach cone sketched in Fig. 1.

Figure 2.5 can be used, for instance, to solve the supersonic flow over a wedge, characterized by the appearance of an oblique shock, that forms an angle  $\theta$  with the wall, deflecting the incoming stream to make it parallel to the wedge, as sketched in Fig. 2.7. If the incident Mach number is  $M_1 = 2$  and the wedge semi angle is  $\delta = 15^\circ$ , then two solutions are possible, as can be seen in Fig. 2.5. Following the arguments given above, we select the weaker shock, corresponding to  $\beta \simeq 45^\circ$ , thereby giving  $\theta = \beta - \delta = 30^\circ$  and  $M_{1n} = M_1 \sin \beta = \sqrt{2}$ . Using now (2.25) and (2.26) yields  $p_2/p_1 \simeq 2.17$  and  $M_{2n} \simeq 0.734$ . This last value can be substituted into (2.38) to give  $M_2 = 1.47$ . The problem could also be solved by using Fig. 2.6 instead, an exercise left for the reader to attempt. Also of interest is that, for the flow over a wedge, no solution involving an oblique shock exists for  $\delta > \delta_{\max} \simeq 23^\circ$ . In that case, the shock detaches to form a bow shock wave, which is locally planar at the center line and becomes increasingly inclined farther away. These bow shock waves are found in general in front of blunt bodies, as seen in the experimental visualization shown below in Fig. 2.8.

Regarding the flow over a wedge (or rather the equivalent case of the flow around a concave corner), it is of interest to consider what happens when, instead of a sharp corner, one encounters a smoothly curved wall, as shown in Fig. 2.9. The perturbations associated with the continuous increase of slope are necessarily weak near the wall, and therefore give rise to a system of Mach waves that propagate into the stream with a local angle of incidence  $\beta = \mu$  such that, at each position,  $M_n = M \sin \beta = 1$ . For the concave wall, the value of  $M$  decreases and the pressure increases as the flow crosses the system of Mach waves, giving an increasing value of  $\mu$  and causing the Mach waves to approach one another. The compression reinforces as a result of the interaction between the different Mach waves, so that a shock wave of finite strength eventually emerges. This complex interaction process is at the origin of the oblique shock that is seen to



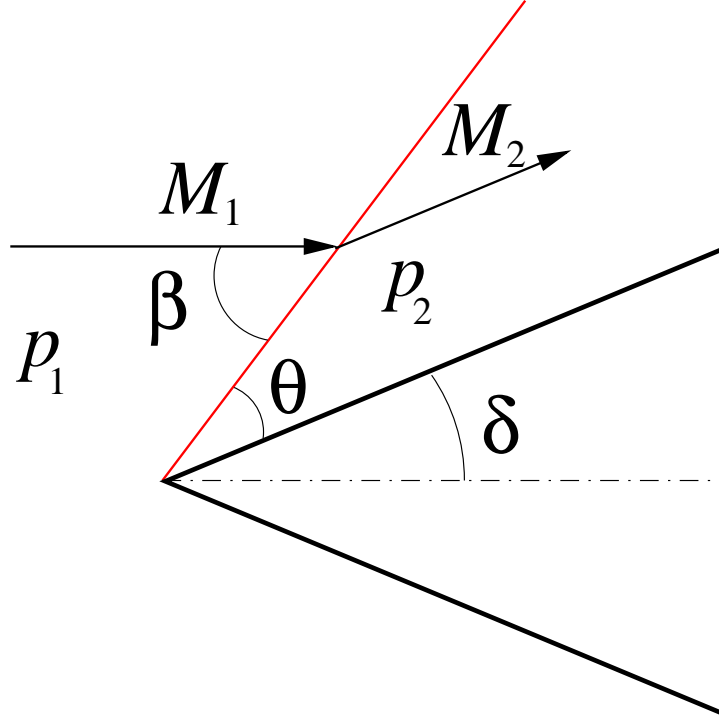


Figure 2.7: Supersonic flow over a wedge.

emerge from the corner when the observation distance is sufficiently large for the curved wall to appear as a sharp corner (see Fig. 2.9).

## Prandtl-Meyer expansions

Let us now consider the case of supersonic flow over a convex wall, represented in Fig. 2.10. A system of Mach waves originates from the wall as it curves downwards. In this case, however, the value of  $M$  increases and the pressure decreases as the flow crosses the system of Mach waves, giving an decreasing value of  $\mu$  and causing the Mach waves to open up. As a result, the expansion wave generated as the supersonic stream turns around the convex corner is formed by a fan of Mach waves that cause the stream lines to evolve smoothly. Since the resulting flow is steady and isentropic, all stagnation magnitudes are preserved across the expansion wave.

Besides the condition of conservation of all stagnation properties,

$$\frac{T_0}{T} = \left(\frac{p_0}{p}\right)^{(\gamma-1)/\gamma} = \left(\frac{\rho_0}{\rho}\right)^{\gamma-1} = \left(\frac{a_0}{a}\right)^2 = 1 + \frac{\gamma-1}{2}M^2, \quad (2.40)$$

the solution for the convex-corner expansion, commonly known as Prandtl-Meyer expansion, requires knowledge of the relationship between the flow deflection and the flow acceleration, which comes from consideration of the infinitesimal evolution due to a given Mach wave. As shown schematically in Fig. 2.11, the condition that the tangential component of the velocity

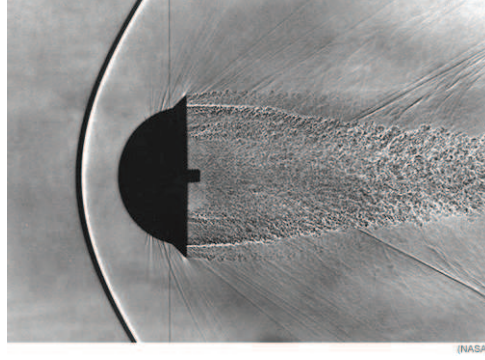


Figure 2.8: Supersonic flow over a blunt body.

must be conserved as the flow is deflected can be used to relate the velocity increment and the deflection according to

$$d\theta = \frac{dv/\tan \mu}{v}. \quad (2.41)$$

From (2.39) it follows that

$$\tan \mu = \frac{1}{\sqrt{M^2 - 1}}. \quad (2.42)$$

To obtain  $dv/v$  we begin by differentiating  $v = Ma$  to give

$$\frac{dv}{v} = \frac{dM}{M} + \frac{da}{a}. \quad (2.43)$$

On the other hand, differentiating the last equation in (2.40) for a constant value of  $a_0$  yields

$$\frac{da}{a} = -\frac{1}{2} \frac{(\gamma - 1)M dM}{1 + (\gamma - 1)M^2/2}, \quad (2.44)$$

which can be combined with (2.43) to provide

$$\frac{dv}{v} = \frac{1}{1 + (\gamma - 1)M^2/2} \frac{dM}{M}. \quad (2.45)$$

Substituting (2.42) and (2.45) into (2.41) finally gives

$$d\theta = \frac{\sqrt{M^2 - 1}}{1 + (\gamma - 1)M^2/2} \frac{dM}{M} \quad (2.46)$$

as a relationship between the deflection and the Mach number increment.

This last equation can be integrated to relate the total deflection  $\theta$  with the change in Mach number as the supersonic stream in Fig. 2.10 turns around the corner according to

$$\theta = \int_{M_1}^{M_2} \frac{\sqrt{M^2 - 1}}{1 + (\gamma - 1)M^2/2} \frac{dM}{M}, \quad (2.47)$$

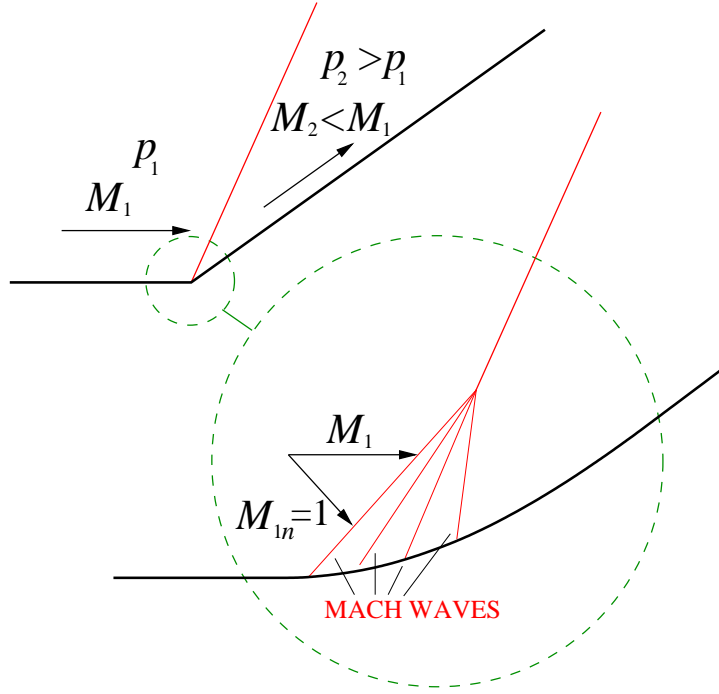


Figure 2.9: Supersonic flow over a concave wall.

which can be alternatively written as

$$\theta = \nu(M_2) - \nu(M_1) \quad (2.48)$$

in terms of the so-called Prandtl-Meyer function

$$\nu(M) = \int_1^M \frac{\sqrt{M^2 - 1}}{1 + (\gamma - 1)M^2/2} \frac{dM}{M} \quad (2.49)$$

given in explicit form by

$$\nu(M) = \sqrt{\frac{\gamma + 1}{\gamma - 1}} \tan^{-1} \left[ \sqrt{\frac{\gamma - 1}{\gamma + 1}} (M^2 - 1) \right] - \tan^{-1}(\sqrt{M^2 - 1}) \quad (2.50)$$

with  $\tan^{-1}$  representing the arctangent (the inverse of the tangent function).

For the problem represented in Fig. 2.10, if the corner angle  $\theta$  and the Mach number of the incoming stream  $M_1$  are known, then one may use (2.48) to determine the value of  $M_2$  and then use (2.40) written in the form

$$\frac{T_2}{T_1} = \left( \frac{p_2}{p_1} \right)^{(\gamma-1)/\gamma} = \left( \frac{\rho_2}{\rho_1} \right)^{\gamma-1} = \left( \frac{a_2}{a_1} \right)^2 = \frac{1 + (\gamma - 1)M_1^2/2}{1 + (\gamma - 1)M_2^2/2} \quad (2.51)$$

to obtain the ratios of thermodynamic properties across the expansion. For instance, if  $\theta = 15^\circ$  and  $M_1 = 2$ , then  $\nu(M_1) = 26.38^\circ$ . Using this value in (2.48) gives  $\nu(M_2) = 41.38^\circ$ , which can be employed to obtain from (2.50) the value  $M_2 \simeq 2.6$ .



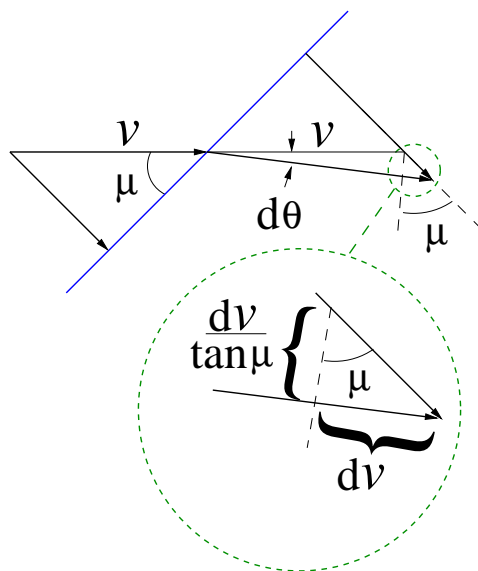


Figure 2.11: Differential evolution across a Mach wave.

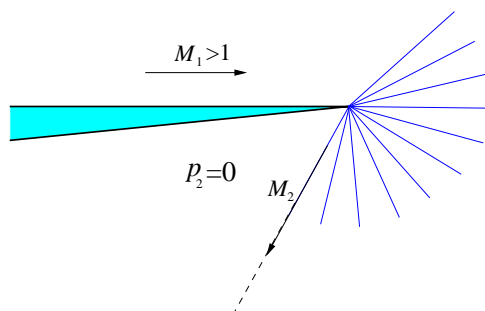


Figure 2.12: Supersonic stream discharging to the vacuum.

## Chapter 3

# Nozzle Flow

### Quasisteady ideal gas flow in pipes

For the large values of the Reynolds number typically found in nozzles, the flow is ideal. For steady operation with negligible body forces the energy and momentum equations can be projected along a given streamline to give

$$\frac{\partial s}{\partial l} = 0 \quad \text{and} \quad \frac{\partial}{\partial l} \left( h + \frac{v^2}{2} \right) = 0, \quad (3.1)$$

indicating that the entropy  $s$  and the sum  $h + v^2/2$  remain constant, i.e.,

$$s = s_0, \quad (3.2)$$

and

$$h + \frac{v^2}{2} = h_0. \quad (3.3)$$

If the nozzle is fed from a container with uniform thermodynamic properties  $s_c$  and  $h_c$ , we may evaluate the above expressions by following the streamline upstream into the container to yield  $s_0 = s_c$  and  $h_0 = h_c$ .

Since the nozzles are slender, in that the ratio of their length  $L$  and characteristic diameter  $D$  satisfies  $L/D \gg 1$ , the resulting streamlines are aligned, with longitudinal and transverse velocity components  $v_T/v_L \sim D/L \ll 1$ , as follows from the continuity equation. Correspondingly, the characteristic changes of pressure across the nozzle section  $\delta_T p \sim \rho_c v_T^2$  are much smaller than the characteristic pressure variation along the nozzle  $\delta_L p \sim \rho_c v_L^2$  according to  $\delta_T p / \delta_L p \sim (D/L)^2 \ll 1$ , so that one may assumed that the pressure remains uniform across each pipe cross section. With  $s = s_c$  everywhere in the pipe and with  $p = p(x)$ , where  $x$  is the distance measured along the nozzle, it is clear that all other thermodynamic variables (e.g.,  $h = h(s, p)$ ,  $T = T(s, p)$ ,  $\rho = \rho(s, p), \dots$ ) are also only a function of  $x$ . For instance,  $h(s, p) = h(s_c, p(x)) = h(x)$ . This last result can be used in (3.3) to demonstrate that  $v = v(x)$ .

In view of the above considerations, the solution can be determined from (3.2) and (3.3) together with

$$G = \rho(x)v(x)A(x), \quad (3.4)$$

where  $G$  is the constant mass flow rate circulating in the pipe. Equations (3.2) and (3.3) can be written with use made of the equations of state in terms of the different stagnation flow variables, according to

$$\frac{h_0}{h(x)} = \frac{T_0}{T(x)} = \left( \frac{a_0}{a(x)} \right)^2 = \left( \frac{p_0}{p(x)} \right)^{(\gamma-1)/\gamma} = \left( \frac{\rho_0}{\rho(x)} \right)^{\gamma-1} = 1 + \frac{\gamma-1}{2} M(x)^2, \quad (3.5)$$

where  $h_0 = h_c$ ,  $T_0 = T_c$ ,  $a_0 = a_c$ ,  $p_0 = p_c$ , and  $\rho_0 = \rho_c$  can be evaluated from the container properties. Similarly, it is convenient to rewrite (3.4) in term of the local Mach number  $M(x)$  to give

$$G = \rho_0 a_0 A(x) M(x) \left( 1 + \frac{\gamma-1}{2} M(x)^2 \right)^{-\frac{\gamma+1}{2(\gamma-1)}}. \quad (3.6)$$

## Subsonic and supersonic flow in pipes

It is of interest to comment on the effect of the Mach number on the character of the fluid motion. For liquid flow in a pipe of varying cross section, our intuition tells us that as the cross section decreases the velocity must increase to accommodate the constant volume flux  $Q = v(x)A(x)$ , while the corresponding pressure  $p(x)$  must decrease to provide the needed acceleration, as follows from Bernoulli's equation  $p + \rho_o v^2/2 = \text{constant}$ . Things are not always quite so intuitive for gas flow, for which the resulting behavior depends on whether the flow is subsonic or supersonic. To see how changes in cross-section area affect the acceleration, we begin by differentiating (3.4) to give

$$\frac{1}{\rho} \frac{d\rho}{dx} + \frac{1}{v} \frac{dv}{dx} = -\frac{1}{A} \frac{dA}{dx}. \quad (3.7)$$

On the other hand, for a perfect gas, the condition of isentropic flow (3.2) gives

$$\frac{p}{\rho^\gamma} = \frac{p_0}{\rho_0^\gamma}, \quad (3.8)$$

providing

$$\frac{1}{\rho} \frac{d\rho}{dx} = \frac{1}{a^2} \frac{1}{\rho} \frac{dp}{dx} \quad (3.9)$$

upon differentiation, with  $a^2 = \gamma p/\rho$ . Since

$$\frac{1}{\rho} \frac{dp}{dx} = \frac{dh}{dx} \quad (3.10)$$

as follows from the condition of isentropic flow  $Tds = dh - dp/\rho = 0$  and with

$$\frac{dh}{dx} = -v \frac{dv}{dx}, \quad (3.11)$$

obtained by differentiating (3.3), (3.7) finally yields

$$(1 - M^2) \frac{1}{v} \frac{dv}{dx} = -\frac{1}{A} \frac{dA}{dx}. \quad (3.12)$$

For subsonic flow ( $M < 1$ ) along a convergent nozzle ( $dA/dx < 0$ ) the velocity increases, as can be seen from (3.12), and the enthalpy, temperature, pressure, density, and velocity of sound decrease, as seen in (3.5) and (3.11). With  $v$  increasing and  $a$  decreasing the associated Mach number  $M = v/a$  continuously increases as the cross section decreases. Because of the presence of the factor  $(1 - M^2)$  in (3.12) the opposite behavior is found for supersonic flow in a convergent nozzle, that is, the flow decelerates and the Mach number decreases, while  $h$ ,  $T$ ,  $p$ ,  $\rho$ , and  $a$  increase. It is therefore not possible to accelerate a subsonic stream beyond sonic conditions with use made of a convergent nozzle.

Observation of (3.12) reveals that a divergent nozzle ( $dA/dx > 0$ ) is required to accelerate a supersonic flow. It also indicates that, if sonic conditions  $M = 1$  are reached at a given section  $x$ , at that location the cross-section area must satisfy  $dA/dx = 0$ . These findings suggest that supersonic flow can be therefore achieved by utilizing a convergent-divergent nozzle so that the flow accelerates through the converging stretch to reach sonic conditions at the throat (the section of minimum area), further accelerating downstream into the supersonic regime in the diverging stretch. We shall see that, depending on the conditions, the flow in convergent-divergent nozzles may include a number of complicating features, including shock and expansion waves, to be treated in a later chapter.

## Critical magnitudes

For steady gas flow in a pipe (3.5) provides the variation of the different thermodynamic variables with  $M$ . It can be used to determine, for instance, their critical values

$$\frac{h_0}{h^*} = \frac{T_0}{T^*} = \left(\frac{a_0}{a^*}\right)^2 = \left(\frac{p_0}{p^*}\right)^{(\gamma-1)/\gamma} = \left(\frac{\rho_0}{\rho^*}\right)^{\gamma-1} = \frac{\gamma+1}{2}. \quad (3.13)$$

found at a section where the flow is sonic. At that critical section, (3.6) provides

$$G = G^* = \rho_0 a_0 A^* \left(\frac{\gamma+1}{2}\right)^{-\frac{\gamma+1}{2(\gamma-1)}}, \quad (3.14)$$

which can be written in the form

$$\frac{A}{A^*} = \frac{1}{M} \left[ \frac{2}{\gamma+1} \left( 1 + \frac{\gamma-1}{2} M^2 \right) \right]^{\frac{\gamma+1}{2(\gamma-1)}} \quad (3.15)$$

thereby relating the values of  $A$  and  $M$  found at a given section with the area  $A^*$  of the section where sonic conditions would be attained.

## Flow in a convergent nozzle

We begin by analyzing the discharge of a gas container with known gas properties ( $p_c$ ,  $\rho_c$ ,  $T_c$ ,  $a_c$ , ...) through a convergent nozzle of minimum cross section  $A(L)$  at the outlet  $x = L$  into a surrounding gas atmosphere at ambient pressure  $p_a$ . The solution, depending on the thermodynamic properties in the container and on the ambient pressure  $p_a$ , can be determined with use made of (3.5) and (3.6) with  $T_0 = T_c$ ,  $a_0 = a_c$ ,  $p_0 = p_c$ , and  $\rho_0 = \rho_c$ . An outflow



is established whenever  $p_a < p_c$ . The flow is strongly subsonic for small pressure differences  $p_c - p_a \ll p_c$ , when the gas discharges into the outer atmosphere as a low-Mach-number jet with pressure  $p(L) = p_a$  at the exit section  $x = L$ . This last condition enables the Mach number  $M(L)$  to be computed from (3.5) according to

$$\left(\frac{p_c}{p_a}\right)^{(\gamma-1)/\gamma} = 1 + \frac{\gamma-1}{2}M(L)^2 \quad \rightarrow \quad M(L) = \left(\frac{2}{\gamma-1}\right)^{1/2} \left[\left(\frac{p_c}{p_a}\right)^{(\gamma-1)/\gamma} - 1\right]^{1/2}, \quad (3.16)$$

to be substituted into (3.6) to determine the gas flow rate through the nozzle

$$G = \rho_c a_c A(L) \left(\frac{2}{\gamma-1}\right)^{1/2} \left(\frac{p_c}{p_a}\right)^{-\frac{\gamma+1}{2\gamma}} \left[\left(\frac{p_c}{p_a}\right)^{\frac{\gamma-1}{\gamma}} - 1\right]^{1/2}. \quad (3.17)$$

As the value of  $p_c/p_a$  increases so does the value of  $M(L)$  given by (3.16) and also the value of  $G$  given by (3.17), with variations given in Fig. 3.1 for  $\gamma = 1.4$ . Using the value of  $G$ , computed for a given value of  $p_c/p_a$  from (3.17), in (3.6) enables the Mach number distribution to be obtained along the nozzle, whereas (3.5) provides the accompanying distributions of pressure, density, and temperature. Sample schematic profiles are given in Fig. 3.2.

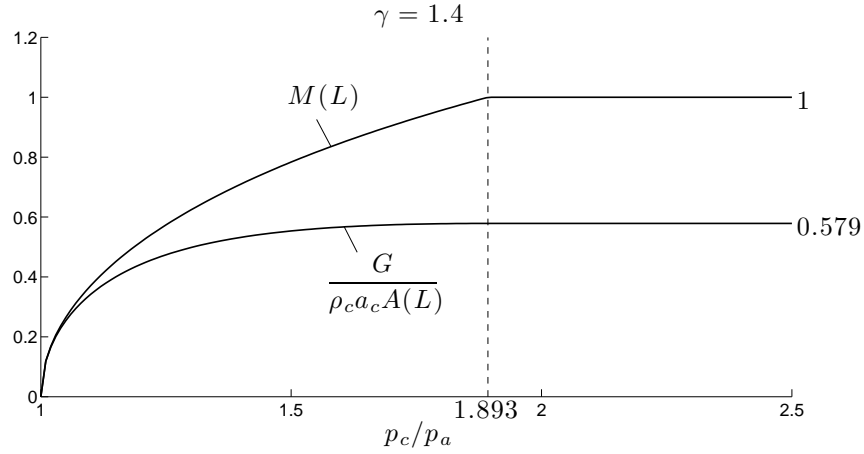


Figure 3.1: The variation of the exit Mach number  $M(L)$  and mass flow rate  $G$  with  $p_c/p_a$  as obtained from (3.16) and (3.17) for  $\gamma = 1.4$ .

As discussed above, the Mach number at the exit section increases for increasing values of  $p_c/p_a$ . The jet solution with  $p(L) = p_a$  and the computation procedure described above continue to hold as long as  $p_a$  remains above a critical choking value  $p_{CH}$  at which the flow reaches sonic conditions at the outlet section. This choking value is determined from (3.16) with  $M(L) = 1$  as

$$\frac{p_c}{p_{CH}} = \left(\frac{\gamma+1}{2}\right)^{\gamma/(\gamma-1)} \quad (3.18)$$

giving  $p_c/p_{CH} \simeq 1.893$  for  $\gamma = 1.4$  ( $p_{CH} \simeq 0.53p_c$ ). For these choking conditions the mass flow

rate reaches the critical value  $G^*$

$$G^* = \rho_c a_c A(L) \left( \frac{\gamma + 1}{2} \right)^{-\frac{\gamma+1}{2(\gamma-1)}}, \quad (3.19)$$

given in (3.14). The flow cannot accelerate past sonic conditions in the convergent nozzle by decreasing the ambient pressure. Instead, the solution becomes choked, that is, for values of  $p_a < p_{CH}$  the flow is sonic at the exit, and becomes independent of the outer pressure<sup>1</sup>. In particular, the mass flow rate, which for  $p_a > p_{CH}$  increases for increasing values of  $p_c/p_a$ , remains equal to  $G^*$ , independent of  $p_a$ , for  $p_a < p_{CH}$ . In the choked flow that emerges for  $p_c/p_a > [(\gamma + 1)/2]^{\gamma/(\gamma-1)}$ , the condition  $M(L) = 1$  therefore replaces  $p(L) = p_a$ . The pressure at the exit section is  $p(L) = p_{CH} > p_a$ , so that the jet flow with parallel streamlines found downstream from the pipe outlet for  $p_a > p_{CH}$  is replaced for  $p_a < p_{CH}$  by a complicated flow pattern including expansion waves that deflect the streamlines outwards.

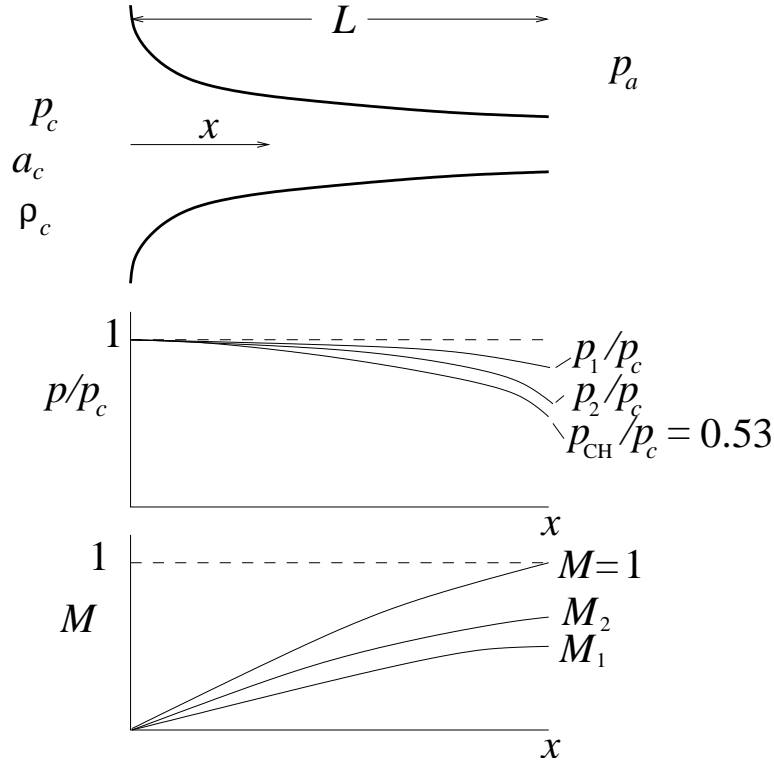
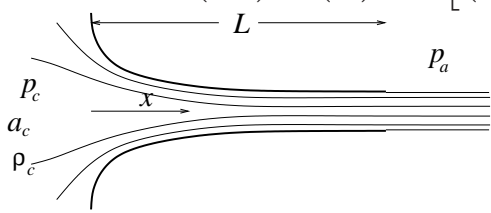
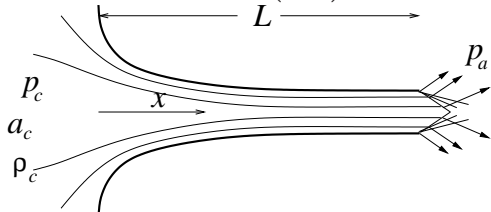


Figure 3.2: Pressure and Mach number distributions along a nozzle for different values of  $p_a/p_c$ .

In summary, the discharge of a container of pressure  $p_c$  into the atmosphere, at pressure  $p_a$ , through a convergent nozzle of minimum cross section  $A(L)$  depends on the value of  $p_c/p_a$ , so that

<sup>1</sup>Note that the decrease of the ambient pressure below  $p_{CH}$  cannot be “felt” within the nozzle, because the flow at the exit is already sonic, and therefore the perturbations cannot travel upstream, so that for  $p_a < p_{CH}$  the flow in the nozzle becomes independent of  $p_a$ .

If $\frac{p_c}{p_a} \leq \left(\frac{\gamma+1}{2}\right)^{\gamma/(\gamma-1)}$ :	$p(L) = p_a$ $M(L) = \left(\frac{2}{\gamma-1}\right)^{1/2} \left[ \left(\frac{p_c}{p_a}\right)^{(\gamma-1)/\gamma} - 1 \right]^{1/2} \leq 1$ $G = \rho_c a_c A(L) \left(\frac{2}{\gamma-1}\right)^{1/2} \left(\frac{p_c}{p_a}\right)^{-\frac{\gamma+1}{2\gamma}} \left[ \left(\frac{p_c}{p_a}\right)^{\frac{\gamma-1}{\gamma}} - 1 \right]^{1/2}$ 
If $\frac{p_c}{p_a} > \left(\frac{\gamma+1}{2}\right)^{\gamma/(\gamma-1)}$ :	$M(L) = 1$ $p(L) = p_{CH} = \left(\frac{\gamma+1}{2}\right)^{-\gamma/(\gamma-1)} p_c > p_a$ $G = G^* = \rho_c a_c A(L) \left(\frac{\gamma+1}{2}\right)^{-\frac{\gamma+1}{2(\gamma-1)}}$ 

## Flow in convergent-divergent nozzles

The flow in convergent-divergent nozzles is more complicated. The nozzle geometry is defined by the values of the exit area  $A_e$  and throat area  $A_t$  (the section of minimum cross-section area). The nozzle is assumed to be connected to a reservoir, where the gas pressure is  $p_0$ , and discharges to the atmosphere, where the pressure is  $p_a$ . Different solutions emerge depending on the value of  $p_a/p_0$ , as indicated in Fig. 3.3.

Let us begin by considering the case where the ambient pressure is only slightly smaller than  $p_0$  (case *a* in Fig. 3.3). As a result of the pressure difference, there appears a slow isentropic steady outflow. For the resulting subsonic flow, the pressure decreases as the Mach number increases in the convergent part of the nozzle, and opposite behaviors are observed in the divergent stretch. The minimum pressure and the maximum Mach number are therefore reached at the throat. The flow discharges to the ambient as a subsonic jet. The condition that the pressure at the exit equals the ambient value can be used to compute the Mach at the exit section from

$$\left(\frac{p_0}{p_a}\right)^{(\gamma-1)/\gamma} = 1 + \frac{\gamma-1}{2} M_e^2, \quad (3.20)$$

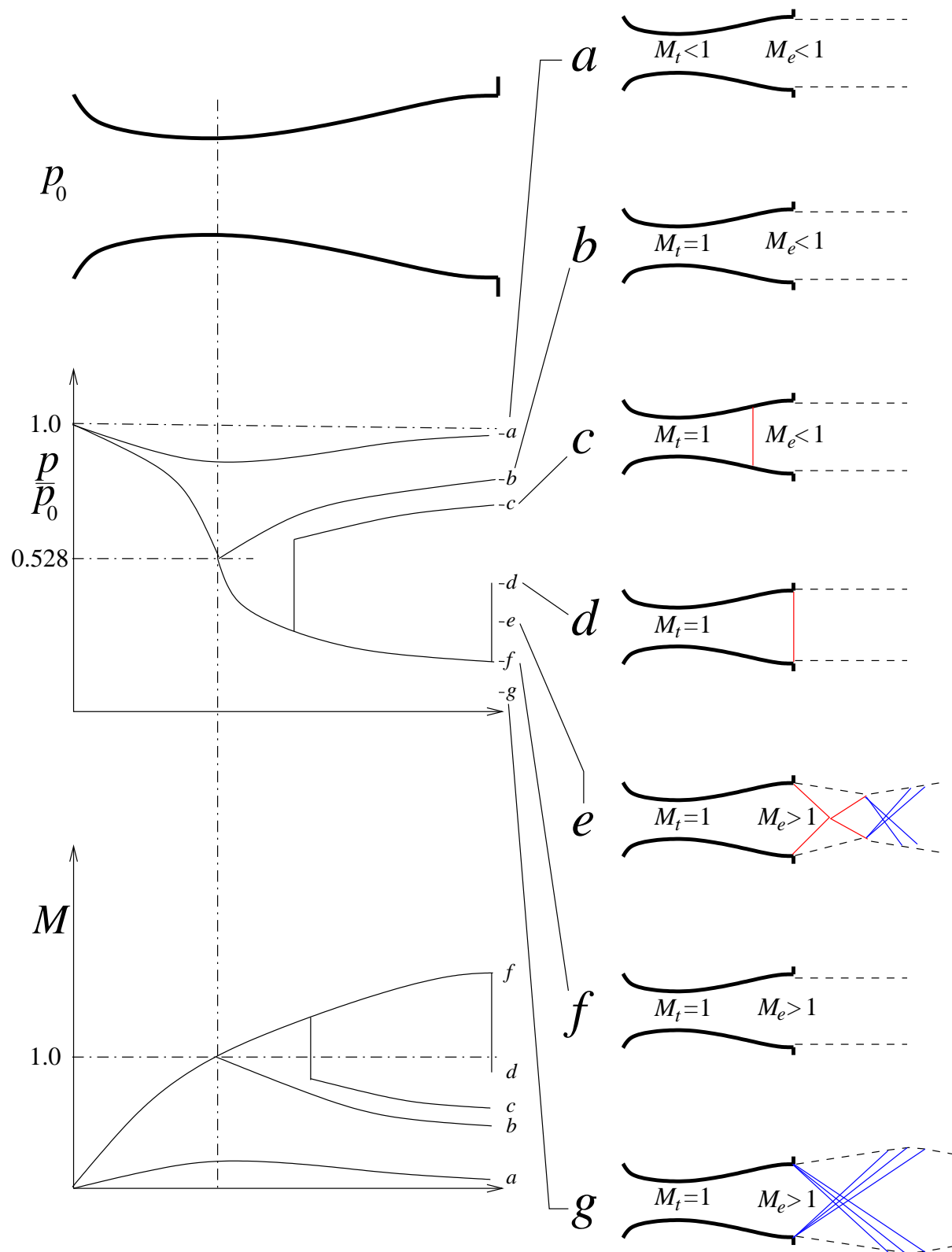


Figure 3.3: Flow in a convergent-divergent nozzle.

which in turn determines the mass flow rate

$$\begin{aligned} G &= \rho_0 a_0 A_e M_e \left( 1 + \frac{\gamma-1}{2} M_e^2 \right)^{-\frac{\gamma+1}{2(\gamma-1)}} \\ &= \rho_0 a_0 A_e \left( \frac{2}{\gamma-1} \right)^{1/2} \left( \frac{p_0}{p_a} \right)^{-\frac{\gamma+1}{2\gamma}} \left[ \left( \frac{p_0}{p_a} \right)^{\frac{\gamma-1}{\gamma}} - 1 \right]^{1/2}, \end{aligned} \quad (3.21)$$

with the stagnation properties for the flow being those found in the reservoir. The Mach number at the throat  $M_t > M_e$  can be obtained from

$$A_e M_e \left( 1 + \frac{\gamma-1}{2} M_e^2 \right)^{-\frac{\gamma+1}{2(\gamma-1)}} = A_t M_t \left( 1 + \frac{\gamma-1}{2} M_t^2 \right)^{-\frac{\gamma+1}{2(\gamma-1)}} \quad (3.22)$$

obtained by equating the values of  $G$  evaluated at the throat

$$G = \rho_0 a_0 A_t M_t \left( 1 + \frac{\gamma-1}{2} M_t^2 \right)^{-\frac{\gamma+1}{2(\gamma-1)}} \quad (3.23)$$

and at the exit.

The value of  $M_t$  continues to increase for decreasing values of  $p_a/p_0$ , reaching sonic conditions when  $p_a = p_{\text{CH}}$  (case *b* in Fig. 3.3). The value of  $p_{\text{CH}}/p_0$  can be determined as a function of  $A_t/A_e$  by equating the mass flow rate at the throat,

$$G = \rho_0 a_0 A_t \left( \frac{\gamma+1}{2} \right)^{-\frac{\gamma+1}{2(\gamma-1)}} \quad (3.24)$$

evaluated from (3.23) with  $M_t = 1$ , to that crossing the exit section, evaluated from (3.21), yielding

$$\frac{A_t}{A_e} = \left( \frac{\gamma+1}{2} \right)^{\frac{\gamma+1}{2(\gamma-1)}} \left( \frac{2}{\gamma-1} \right)^{1/2} \left( \frac{p_0}{p_a} \right)^{-\frac{\gamma+1}{2\gamma}} \left[ \left( \frac{p_0}{p_a} \right)^{\frac{\gamma-1}{\gamma}} - 1 \right]^{1/2}. \quad (3.25)$$

It can be seen that, for a given value of  $A_t/A_e$ , this last equation is satisfied by two different values of  $p_a/p_0$ . One of the two solutions, corresponding to the choking value  $p_a = p_{\text{CH}}$ , is associated with an exit Mach number  $M_e < 1$ , to be evaluated from (3.20) with  $p_a = p_{\text{CH}}$ . There exists, however, a second isentropic solution with  $p_a < p_{\text{CH}}$  in which the flow discharges as a supersonic jet with  $p_e = p_a = p_{\text{SJ}}$  and  $M_e > 1$ . For instance, for  $A_t/A_e = 0.477$  the two solutions of (3.25) and (3.20) are  $p_a/p_0 = p_{\text{CH}}/p_0 = 0.943$  with  $M_e = 0.29$  and  $p_a/p_0 = p_{\text{SJ}}/p_0 = 0.0865$  with  $M_e = 2.25$ .

The results indicate that the convergent-divergent nozzle can be choked more easily than the convergent nozzle (note that for  $A_t/A_e = 0.477$  a value  $p_a/p_0 = 0.943$  is sufficient to choke the flow, to be compared with the value  $p_a/p_0 = 0.528$  required in convergent nozzles). The flow remains choked for  $p_a < p_{\text{CH}}$ , which implies that, regardless of the value of  $p_a$ , the flow in the convergent part of the nozzle is identical, with the mass flow rate taking always the constant value (3.24). In the isentropic solution discharging as a supersonic jet (case *f* in Fig. 3.3) the flow is therefore subsonic in the convergent stretch, sonic at the throat, and supersonic in the

divergent stretch, leaving the nozzle with  $p_e = p_a$ , so that neither expansions nor compressions are needed to adapt the pressure to the ambient value.

It is of interest to consider what happens when the ambient pressure is below  $p_{SJ}$  and also when it takes intermediate values in the range  $p_{SJ} < p_a < p_{CH}$ . For  $p_a < p_{SJ}$  (case *g* in Fig. 3.3), the flow conditions at the exit are exactly those found for  $p_a = p_{SJ}$ , so that  $p_e = p_{SJ} > p_a$  (underexpanded flow). An expansion is therefore needed outside the nozzle to decrease the pressure to the ambient value. The expansion wave that appears is locally planar near the nozzle rim and therefore corresponds there to a Prandtl-Meyer expansion, which deflects the stream outwards as it decreases its pressure to  $p_a$  while increasing its Mach number beyond that found at the exit section.

Similarly, when the ambient pressure is slightly above  $p_{SJ}$  (case *e* in Fig. 3.3), the flow conditions at the exit are also exactly those found for  $p_a = p_{SJ}$ . In this case, however, the flow is overexpanded, and a shock wave is needed to increase the pressure to the ambient value. When  $p_a$  is only slightly above  $p_{SJ}$ , an oblique weak shock is sufficient. As the value of  $p_a$  further increases, the needed shock wave becomes stronger, and the associated incidence angle increases towards  $\beta = \pi/2$ . There is a critical value of  $p_a$  for which the compression occurs through a normal shock wave standing at the exit section (case *d* in Fig. 3.3). For even larger values of  $p_a$  the shock wave migrates into the divergent stretch of the nozzle, so that downstream from the throat there is a region of supersonic flow that ends at the inner shock, which is followed by a region of subsonic flow eventually discharging to the ambient as a jet, as indicated in Fig. 3.3. These steady solutions including planar shock waves within the divergent part of the nozzle are hard to observe in reality, because they are often affected by boundary-layer separation immediately downstream from the shock, which may lead to significant changes in the downstream flow structure, including at times unsteady flow variations and asymmetric flow patterns.